Novel *CYP1B1-RMDN2* Alzheimer's disease locus identified by genome-wide association analysis of cerebral tau deposition on PET

Kwangsik Nho[1,2,3,4*], Shannon L. Risacher[1,3*], Liana Apostolova[1,3,5,6], Paula J. Bice[1,3], Jared Brosch[3,5], Rachael Deardorff[3,5], Kelley Faber[6,7], Martin R. Farlow[3,5], Tatiana Foroud[3,6,7], Sujuan Gao[3,8], Thea Rosewood[1,2,3], Jun Pyo Kim[1,2,3], Kelly Nudelman[3,6,7], Paul Aisen[9], Reisa Sperling[10], Basavaraj Hooli[11], Sergey Shcherbinin[11], Diana Svaldi[11], Clifford R. Jack[12], William J. Jagust[13], Susan Landau[13], Aparna Vasanthakumar[14], Jeffrey F. Waring[14], Vincent Doré[15,16], Simon M. Laws[17], Colin L. Masters[18], Tenielle Porter[17], Christopher C. Rowe[16], Victor L Villemagne[16,19], Logan Dumitrescu[20], Timothy J. Hohman[20,21], Julia B. Libby[20], Elizabeth Mormino[22], Rachel F. Buckley[10], Keith Johnson[10,23], Hyun-Sik Yang[10,24], Ronald C. Petersen[25], Vijay K. Ramanan[25], Prashanthi Vemuri[12], Ann D. Cohen[19], Kang-Hsien Fan[26], M. Ilyas Kamboh[26], Oscar L. Lopez[19,27], David A. Bennett[28], Muhammad Ali[29], Tammie Benzinger[30], Carlos Cruchaga[29,31], Diana Hobbs[30], Philip L. De Jager[32], Masashi Fujita[32], Vaishnavi Jadhav[6,33], Bruce T. Lamb[3,6,33], Andy P. Tsai[33,34], Isabel Castanho[35,36], Jonathan Mill[35], Michael W. Weiner[37,38], for the Alzheimer's Disease Neuroimaging Initiative (ADNI)[§], the Alzheimer's Disease Neuroimaging Initiative – Department of Defense[§], the Anti-Amyloid Treatment in Asymptomatic Alzheimer's Study (A4 Study)[§], and the Australian Imaging, Biomarker & Lifestyle Study (AIBL)[§], Andrew J. Saykin[1,2,3,5,6¥]

[1]*Center for Neuroimaging, Department of Radiology and Imaging Sciences, Indiana University School of Medicine, Indianapolis, IN, USA;*

[2]*Center for Computational Biology and Bioinformatics, Indiana University School of Medicine, Indianapolis, IN, USA;*

[3]*Indiana Alzheimer's Disease Research Center, Indiana University School of Medicine, Indianapolis, IN, USA;*

[4]*Department of BioHealth Informatics, Indiana University-Purdue University, Indianapolis, IN, USA;*

[5]*Department of Neurology, Indiana University School of Medicine, Indianapolis, IN, USA;*

[6]*Department of Medical and Molecular Genetics, Indiana University School of Medicine, Indianapolis, IN, USA;*

[7]*National Centralized Repository for Alzheimer's Disease and Related Dementias, Indiana University School of Medicine, Indianapolis, IN, USA;*

[8]*Department of Biostatistics, Indiana University School of Medicine, Indianapolis, IN, USA;*

[9]*Department of Neurology, Keck School of Medicine, University of Southern California, San Diego, CA, USA;*

[10]*Department of Neurology, Massachusetts General Hospital, Harvard Medical School, Boston, MA, USA;*

[11]*Eli Lilly and Company, Indianapolis, IN, USA;*

[12]*Department of Radiology, Mayo Clinic, Rochester, MN, USA;*

[13]*UC Berkeley Helen Wills Neuroscience Institute, University of California - Berkeley, Berkeley, CA, USA;*

[14]*Genomics Research Center, AbbVie, North Chicago, Illinois, USA;*

[15]*CSIRO Health and Biosecurity, Melbourne, Australia;*

[16]*Department of Molecular Imaging & Therapy, Austin Health, Heidelberg, VIC, Australia;*

[17]*Centre for Precision Health, School of Medical and Health Sciences, Edith Cowan University, Joondalup, WA, Australia;*

[18]*Florey Institute of Neuroscience and Mental Health and The University of Melbourne, Parkville, VIC, Australia;*

[19]*Department of Psychiatry, University of Pittsburgh School of Medicine, Pittsburgh, PA, USA;*

[20]*Vanderbilt Memory & Alzheimer's Center, Vanderbilt University Medical Center, Nashville, TN, USA;*

[21]*Vanderbilt Genetics Institute, Vanderbilt University Medical Center, Nashville, TN, USA;*

[22]*Department of Neurology & Neurological Sciences, Stanford University, Stanford, CA, USA;*

[23]*Department of Radiology, Massachusetts General Hospital, Harvard Medical School, Boston, MA, USA;*

[24]*Center for Alzheimer's Research and Treatment, Department of Neurology, Brigham and Women's Hospital, Harvard Medical School, Boston, MA, USA;*

[25]*Department of Neurology, Mayo Clinic, Rochester, MN, USA;*

[26]*Department of Human Genetics, University of Pittsburgh, Pittsburgh, PA, USA;*

[27]*Department of Neurology, University of Pittsburgh School of Medicine, Pittsburgh, PA, USA;*

[28]*Department of Neurological Sciences, Rush Medical College, Rush University, Chicago, IL, USA;*

[29]*Department of Psychiatry, Washington University, St. Louis, MO, USA;*

[30]*Department of Radiology, Washington University School of Medicine, St. Louis, MO, USA;*

[31]*NeuroGenomics and Informatics Center, Washington University School of Medicine, St. Louis, MO, USA;*

[32]*Center for Translational and Computational Neuroimmunology, Department of Neurology and Taub Institute for Research on Alzheimer's Disease and the Aging Brain, Columbia University Irving Medical Center, New York, NY, USA;*

[33]*Stark Neuroscience Research Institute, Indiana University School of Medicine, Indianapolis, IN, USA;*

[34]*Wu Tsai Neurosciences Institute, Stanford University School of Medicine, Stanford, CA, USA;*

[35]*Department for Clinical and Biomedical Sciences, University of Exeter Medical School, University of Exeter, UK;*

[36]*Department of Pathology, Beth Israel Deaconess Medical Center, Boston, MA, USA*

Harvard Medical School, Boston, MA, USA;

[37]*Departments of Radiology, Medicine, and Psychiatry, University of California-San Francisco, San Francisco, CA, USA;*

[38]*Department of Veterans Affairs Medical Center, San Francisco, CA, USA*

*These authors contributed equally to this work.

[¥]Please address correspondence to:

Andrew J. Saykin, PsyD

Department of Radiology and Imaging Sciences, Center for Neuroimaging, Indiana University School of Medicine, Indianapolis, IN, USA

Phone: 317-278-6947; Fax: 317-274-1067; E-mail: asaykin@iu.edu

[§]Data used in preparation of this article were obtained from the Alzheimer's Disease Neuroimaging Initiative (ADNI) database (adni.loni.usc.edu), the Anti-Amyloid Treatment in Asymptomatic Alzheimer's Study (A4) and Longitudinal Evaluation of Amyloid Risk and Neurodegeneration (LEARN) studies (https://ida.loni.usc.edu/collaboration/access/appLicense.jsp;jsessionid=2CC9FA6681E2924181B892706F917FEA) and from the Australian Imaging Biomarkers and Lifestyle (AIBL) Study. As such, the investigators within the ADNI, A4, LEARN, and AIBL consortia contributed to the design and implementation of these studies and/or provided data but, unless named, did not participate in analysis or writing of this report. A complete listing of ADNI investigators can be found at: http://adni.loni.usc.edu/wp-content/uploads/how_to_apply/ADNI_Acknowledgement_List.pdf. A complete list of A4 and LEARN investigators can be found at: https://a4study.org/wp-content/uploads/2018/12/A4-Acknowledgements-Journal-Format.pdf. AIBL researchers are listed at www.aibl.csiro.au.

Word Count: 3499/3500

Figures/Tables: 11 Figures, 2 Tables, 7 Supplemental Figures, 12 Supplemental Tables

References: 83 Primary Manuscript, 87 Supplemental

Abstract

Background: Determining the genetic architecture of Alzheimer's disease (AD) pathologies can enhance mechanistic understanding and inform precision medicine strategies. A genome-wide association study (GWAS) of cortical tau quantified by positron emission tomography (PET) was performed.

Method: Participants included 3,136 non-Hispanic White older adults from 12 independent studies (n=1,449 discovery sample; n=1,687 replication sample) spanning preclinical and clinical stages of AD. Genetic variants associated with cortical tau measured using [^{18}F]flortaucipir or [^{18}F]MK-6240 PET were assessed including relevant covariates. Voxel-wise analysis was used to map the topographic distribution of identified associations. Supporting evidence for the identified SNP from gene expression, methylation quantitative trait loci (QTL), and AD mouse data were evaluated.

Findings: Two novel SNPs at the *CYP1B1-RMDN2* (Cytochrome P450 Family 1 Subfamily B Member 1 and Regulator of Microtubule Dynamics 2) locus were associated with tau deposition. The most significant signal was at rs2113389 (p-value=1.37x10^{-8}), which explained 4.3% of the variation in cortical tau, while *APOE4* rs429358 accounted for 3.6%. The minor allele of rs2113389 (T; MAF=0.146) was associated with higher tau and faster cognitive decline. Additive effects, but no interactions, were observed between rs2113389 and diagnosis, *APOE4*, and Aβ positivity. Voxel-wise analysis revealed higher tau in AD-related regions in rs2113389 T-allele carriers. *CYP1B1* was upregulated in the temporal cortex in AD. The rs2113389 T-allele was associated with higher temporal cortex *CYP1B1* expression and methylation levels. Mouse model

studies provided additional functional evidence for a relationship between *CYP1B1* and tau deposition but not Aβ.

Interpretation: The minor allele of rs2113389 may be a risk variant for tau and faster cognitive decline in AD. Further investigation of *CYP1B1* and *RMDN2* is warranted and may provide insight into the genetic basis of cerebral tau and novel pathways for therapeutic development in AD. Studies of multiethnic populations are also needed.

Key words:

Alzheimer's disease; Imaging genetics; tau PET; *RMDN2*; *CYP1B1*

Abbreviations:

AD: Alzheimer's disease; GWAS: genome-wide association study; SNP: single nucleotide polymorphism; CSF: cerebrospinal fluid; PET: positron emission tomography; APOE: apolipoprotein E; ADNI: Alzheimer's Disease Neuroimaging Initiative; ADNI-DoD: ADNI-Department of Defense; IMAS: Indiana Memory and Aging Study; eQTL: expression quantitative

trait loci; SUVR: standard uptake value ratio; FWHM: Full Width at Half Maximum; ROI: region of interest; HRC: Haplotype Reference Consortium; MAF: minor allele frequency; LASSO: Least Absolute Shrinkage and Selection Operator; CEU: Utah residents with Northern and Western European ancestry from the CEPH collection; TSI: Toscani in Italia; MDS: multidimensional scaling; CN: Cognitively normal older adults; MCI: Mild cognitive impairment; RMDN2: Regulator of Microtubule Dynamics 2; CYP1B1: Cytochrome P450 Family 1 Subfamily B Member 1

Introduction

Alzheimer's disease (AD) is a common neurodegenerative disease.[1] Two pathological hallmarks are amyloid-beta (Aβ) plaques and neurofibrillary tau tangles. Measurements of Aβ and tau with positron emission tomography (PET) are commonly employed in research given the proposed amyloid/tau/neurodegeneration (A/T/N) classification criteria.[2]

Genetic factors conferring susceptibility to or protection from AD are important for identifying target biological pathways for drug development and personalized medicine.[3] Large-scale genome-wide association studies (GWAS) using case-control designs have identified risk genes in immune, tau, Aβ, lipid, and other pathways.[4,5] The strongest AD genetic risk locus is *APOE* (apolipoprotein E) ε4 (*APOE4*).[6] Large case-control studies can be limited in that participant neuropathology is typically unknown. Endophenotype studies of *in vivo* neuropathology complement case-control studies by providing information about genetic variants associated with pathology.[7]

Numerous studies have assessed genetic predictors of Aβ PET measures.[8-13] However, most genetic studies of tau have utilized cerebrospinal fluid (CSF) tau measures due to non-availability of large tau PET datasets.[14] One study investigated the association of tau PET with *BIN1*, finding an association between a known *BIN1* risk single nucleotide polymorphism (SNP; rs744373) and greater [^{18}F]flortaucipir PET.[15] Another performed GWAS on tau PET endophenotypes and identified two genetic loci (*PPP2R2B* and *IGF2BP3*). However, this study had limited statistical power due to the modest sample size (n=754) and did not include a replication sample.[16,17]

Here, we performed the largest GWAS of cortical tau on PET to date (n=3,136). We included data from twelve independent cohorts. We also assessed the relationship of the top SNP to cognitive decline and evaluated additive and interaction effects with diagnosis, *APOE4* status, and Aβ

positivity in 1,161 individuals with voxel-wise data. We then used voxel-wise analysis to map the topographic distribution of the top variant effect on tau. We also performed a gene-set enrichment analysis, an analysis of gene expression levels in human brain tissue and single-nucleus RNA-Seq data, a methylation analysis, and an expression quantitative trait loci (eQTL) analysis. Finally, we investigated expression levels of the top gene in tau and Aβ mouse models.[18-20]

Materials and methods

Study participants

The analyses included participants from the Alzheimer's Disease Neuroimaging Initiative (ADNI; http://adni.loni.usc.edu), ADNI-Department of Defense (ADNI-DoD), Indiana Memory and Aging Study (IMAS) of the Indiana ADRC, Avid A05 clinical trial (A05), Anti-Amyloid Treatment in Asymptomatic Alzheimer's (A4) and Longitudinal Evaluation of Amyloid Risk and Neurodegeneration (LEARN) studies, Harvard Aging Brain Study (HABS), University of Pittsburgh Alzheimer's Disease Research Center (UPitt ADRC), Mayo Clinic Study of Aging (MCSA), Memory and Aging Project (MAP) at the Knight Alzheimer's Disease Research Center (Knight-ADRC), the Australian Imaging, Biomarker and Lifestyle Study (AIBL), and the Berkeley Aging Cohort Study (BACS). The discovery sample included ADNI, ADNI-DoD, IMAS, A05, A4, HABS, UPitt ADRC. The replication sample included MCSA, MAP-Knight ADRC, AIBL, and BACS. *Post-hoc* analyses of interactions with diagnosis, *APOE4* status, and Aβ positivity, as well as voxel-wise analyses were performed in 1,161 individuals from ADNI, ADNI-DoD, IMAS, A05, A4, and LEARN, as voxel-wise scan data was available on these individuals. Informed consent was obtained for all participants, and studies were approved by the relevant institutional

review boards. Descriptions of all cohorts, as well as demographics and cognitive performance, are found in the Supplemental information (**Supplemental Tables 1-12**).

Genotyping and imputation

Participants were genotyped using several genotyping platforms. Un-genotyped SNPs were imputed separately in each cohort using the Haplotype Reference Consortium (HRC) data as a reference panel.[21] Before imputation, standard sample and SNP quality control (QC) procedures were performed, as described previously.[22] Furthermore, only non-Hispanic participants of European ancestry by multidimensional scaling analysis were selected.[23] Imputation and QC procedures were performed as described previously.[24]

Statistical analysis

Genome-wide association analysis (GWAS): We confirmed that cortical tau deposition followed a normal distribution after a rank-based inverse normal transformation. Using imputed genotypes, a GWAS of cortical tau was performed using a linear regression model with age, sex, two principal component (PC) factors from population stratification, *APOE4* status, and diagnosis as covariates using PLINK.[25] A conservative threshold for genome-wide significant association ($p<5 \times 10^{-8}$) was employed.[26] QQman was used to generate Manhattan and Q-Q plots, and LocusZoom was used to obtain regional association plots for selected loci.[27]

Gene-set enrichment analysis: Gene-set enrichment analysis was performed using GWAS summary statistics to identify pathways and functional gene sets with significant associations with cortical tau deposition using the GSA-SNP software,[28] as described in the Supplemental information. Enriched pathways with cortical tau levels were defined as those with FDR-corrected p-value<0.05.

Gene-based association analysis: Genome-wide gene-based association analysis was performed using GWAS p-values and the KGG software as described previously[29,30] and in the Supplemental information.

Interaction with diagnosis, *APOE* genotype, and Aβ positivity: The effect of the top identified SNP (rs2113389 – dominant model (CC vs. CT/TT)) and its interaction with diagnosis, *APOE4* status, and Aβ positivity, on global and medial temporal lobe (MTL) tau, which is a primary location of early tau in AD, was assessed as described in the Supplemental information. Different effects by sex were also evaluated using stratified analysis (methods in Supplemental information).

Detailed whole-brain imaging analysis: Tau PET SUVR images (n=1,161) were used in a voxel-wise statistical analysis of the effect of the top identified SNP on tau using SPM12 (www.fil.ion.ucl.ac.uk/spm/) in a *post-hoc* analysis (described in the Supplemental information). A voxel-wise threshold of $p<0.05$ with family-wise error (FWE) adjustment for multiple comparisons was used.

AMP-AD bulk RNA-Seq data in the post-mortem human brain: Pre-processed bulk RNA-Seq data from 1,917 samples were downloaded from the Synapse database (https://www.synapse.org/#!Synapse:syn17115987) of the AMP-AD Consortium[31-35] and analyzed as discussed in the Supplemental information. Procedures for sample collection, post-mortem sample descriptions, tissue and RNA preparation methods, library preparation and sequencing methods, and sample quality controls were previously described.[35] Finally, the eQTLGen[36] consortium database (n=31,684) was used for eQTL of rs2113389 with *CYP1B1* expression in blood.

Single-nucleus RNA-Seq (snRNA-Seq) preprocessing and analysis: Frozen brain tissue specimens (n=479) from the dorsolateral prefrontal cortex were obtained in the Religious Orders Study/Memory and Aging Project (ROSMAP) cohort[37] and processed as described in the Supplemental information. Raw data is available through the AD Knowledge Portal (https://www.synapse.org/#!Synapse:syn31512863). Fifty-five samples were excluded for quality control issues (see Supplementary information).

ADNI DNA methylation data: In ADNI, Illumina EPIC chips (Illumina, Inc., San Diego, CA, USA) were used to profile DNA methylation in 1,920 blood or buffy coats samples including 200 duplicate samples according to the Illumina protocols. A detailed protocol has been published previously[38-40] and briefly described in the Supplemental information. We performed methylation quantitative trait loci (meQTLs) of the top SNP discovered with CpGs in that gene (n=634) using multivariate linear models adjusted for age, sex, cell composition changes, and DNA storage/source.

AD pathology mouse model analysis: hTau mouse model: Generation of the hTAU mice, as well as brain extraction and tissue processing, was described previously[18,19,41,42] and in the Supplemental information. Student's t test was performed for qPCR results comparing C57BL/6J (B6; wild type) and hTAU mice. rTg4510 and J20 mouse model: Transgenic mice harboring human tau (rTg4510) and amyloid precursor protein (J20) mutations were used to investigate if gene expression changes of the top identified gene was associated with AD pathology.[20] The rTg4510 mouse model and J20 mouse models, as well as experimental models and methods, were described previously[20,43-46] and briefly in the Supplemental information. A Wald test was used to assess genotype effects, while a likelihood-ratio test was used to assess significant effects of age

and interaction effects (Genotype*Age) using the DESeq2 package.[47] Associations between gene expression and neuropathology quantified by immunohistochemistry were tested with DESeq using a Wald test to calculate *P*-values. Models were fitted separately for neuropathology data measured in the entorhinal cortex for each mouse. *P*-values were adjusted for multiple testing using false discovery rate (FDR).[48]

Results

Genome-wide association analysis (GWAS)

Additive genetic models were tested for each SNP with transformed cortical tau adjusted for age, sex, two PCs from population stratification analysis, *APOE4* status (presence/absence), and diagnosis. We meta-analyzed GWAS results from seven cohorts in the discovery stage (n=1,449). GWAS results for cortical tau are shown as quantile-quantile (**Figure 1A**) and Manhattan (**Figure 1B**) plots. No evidence of systematic *p*-value inflation was found (genomic inflation factor λ=1.025; **Figure 1A**). We identified a genome-wide significant association of cortical tau with a novel locus at 2p22.2 (**Figure 1B**), with two SNPs in the region reaching genome-wide significance (*p*-value $\leq 5x10^{-8}$). The SNP with the strongest association for cortical tau is rs2113389, which was directly genotyped. The other SNP (rs918804) is in strong linkage disequilibrium (LD, $r^2 = 0.91$ and D' = 0.95) with rs2113389. The SNP (rs2113389) is located on 2p22.2 between *RMDN2* and *CYP1B1* and non-coding RNA, *CYP1B1-AS1* (**Figure 2**). The minor allele T of rs2113389 (MAF=0.146) was associated with higher tau (Z score=5.68; *p*-value=1.37 x 10^{-8}) and remained significant after including Aβ positivity as a covariate. We conducted a replication meta-analysis in five additional cohorts (n=1,687). The genome-wide significant SNPs (rs2113389 and rs918804) in the discovery stage were replicated with the same association

direction (*Z* score=3.83, *p*-value=1.26 x 10^{-4}; Z-score=-2.97, *p*-value=2.97x10^{-3}, respectively) (**Supplemental Figure 1**). When estimating the proportion of variance in cortical tau explained by these genetic variants using the Genome-wide Complex Trait Analysis (GCTA) tool[49], we found that ~4.3% of the variation in cortical tau in ADNI are explained by rs2113389 and *APOE4* SNP rs429328 alone, accounting for 3.6% of variance. In ADNI, rs2113389 was associated with longitudinal decline in executive function over one year after adjustment for age, sex, education, *APOE4* status, and baseline executive function (N=1,466; β=-0.053; *p*-value=0.014). Participants with the minor allele T of rs2113389 showed faster decline relative to non-carriers.

Association of rs2113389 genotype with regional and global tau

Figure 3 shows that both the additive (**Figure 3A&B**) and dominant models (**Figure 3C&D**) demonstrated higher MTL and cortical tau deposition in carriers of the minor allele (T) of rs2113389. Similar results were observed when stratified by sex (**Supplemental Figures 2 & 3**).

Interaction of rs2113389 genotype with variables of interest

Main effects of diagnosis and rs2113389 genotype were observed, with a higher MTL and cortical tau across diagnoses, but there was no interaction effect with rs2113389 dominant genotype (**Figure 4**). The effect was similar in both males and females (**Supplemental Figure 4**). Main effects, but no interaction effect, for rs2113389 genotype and *APOE4* status were also observed (**Figure 5**), with those positive for both *APOE4* and rs2113389 minor allele (T) showing the highest MTL and cortical tau. The sex-stratified analysis showed similar results in both males and females (**Supplemental Figure 5**). Finally, main effects of Aβ positivity and rs2113389 genotype, but no interaction effect, on MTL and cortical tau were observed (**Figure 6**), with Aβ+ carriers of the rs2113389 minor allele (T) showing the highest tau. In the sex-stratified analysis, males and

females showed similar results (**Supplemental Figure 6A,B**), except for an interaction effect of Aβ positivity and rs2113389 genotype on MTL tau deposition in females (**Supplemental Figure 6C**) and a trend for cortical tau (**Supplemental Figure 6D**).

Voxel-wise association of rs2113389 genotype with tau

A voxel-wise analysis of the effect of rs2113389 (voxel-wise $p<0.05$ (FWE corrected), minimum cluster size (k)=100 voxels; **Figure 7** and **Supplemental Figure 7**) was completed to evaluate the topographic pattern of the association. In the dominant model, individuals carrying at least one minor allele at rs2113389 (CT or TT; n=327) demonstrated greater tau throughout the temporal lobe, parietal lobe, and inferior frontal lobe than rs2113389 CC individuals (n=834; **Figure 7A**). Beta-value maps supported the statistical map, showing widespread areas where rs2113389-T carriers show higher tau than non-carriers (**Figure 7B**). Using an additive model, rs2113389 CT individuals (n=300) showed higher tau than CC individuals (n=834) in the temporal, lateral parietal, and frontal lobes (**Supplemental Figure 7A**), while rs2113389 TT (n=27) showed a more focal region of higher frontal tau relative to rs2113389 CC individuals (**Supplemental Figure 7B**). Beta-value maps revealed interesting patterns, with rs2113389 CT individuals showing higher temporal and parietal tau relative to rs2113389 CC individuals (**Supplemental Figure 7C**). Alternatively, rs2113389 TT individuals showed widespread higher tau relative to rs2113389 CC individuals, especially in the frontal lobe (**Supplemental Figure 7D**). Finally, despite not reaching statistical significance likely due to power issues, the beta-values map shows that rs2113389 TT homozygotes show higher frontal tau than rs2113389 CT heterozygotes (**Supplemental Figure 7E**). These findings may suggest later Braak stages are more likely in TT

homozygotes or that TT homozygotes have a cortical rather than limbic pattern relative to CT heterozygotes and CC homozygotes.

Pathway analysis

When gene ontology (GO) terms were considered, 480 gene-sets were significant after correction for multiple testing. GO for cell-cell adhesion was the most significant pathway identified (**Table 1**). GO terms for MHC protein complex, postsynaptic density, regulation of synaptic transmission, and calcium ion transport were also significant. For the Kyoto Encyclopedia of Genes and Genomes (KEGG) pathway, 44 gene-sets were significant, including cell adhesion molecules, calcium signaling pathways, and axon guidance (**Table 2**).

Gene expression analysis and eQTL analysis

Our genome-wide gene-based association analysis identified two protein coding genes (*CYP1B1* (corrected *p*-value=0.040), *RMDN2* (corrected *p*-value=0.040)), and one non-coding RNA (*CYP1B1-AS1* (corrected *p*-value=0.040)) as associated with cortical tau after multiple testing adjustment. Then, bulk RNA-Seq data from 1,917 samples preprocessed in AMP-AD was evaluated for these genes. The two genes are highly expressed in the brain (**Figure 8)**. Differential expression of *RMDN2* was seen in the parahippocampal gyrus (*p*-value=0.004; **Figure 8a**), with down-regulation in AD. *CYP1B1* demonstrated differential expression in the temporal cortex (*p*-value=0.001; **Figure 8b**), with upregulation in AD. We also investigated whether the identified SNPs were associated with expression levels of *CYP1B1* and *RMDN2* (eQTL). The most significantly associated SNP, rs2113389, was associated with *CYP1B1* expression levels in the temporal cortex, but not with *RMDN2* expression. Specifically, the rs2113389 T-allele was associated with higher temporal *CYP1B1* expression (β=0.25; *p*-value=0.02; **Figure 8c**). Finally,

the rs2113389 T-allele was associated with higher *CYP1B1* expression levels in blood from the eQTLGen consortium database (n=31,684; Z score=24.93; *p*-value= 3.6 x 10^{-137}).

Cell type-specific expression and eQTL analysis of CYP1B1

Single-cell expression of *CYP1B1* in ROSMAP single-nucleus RNA-Seq data from the dorsolateral prefrontal cortex showed that fibroblasts (Fib) had the highest expression of the *CYP1B1* gene across all 12 cell types. Among the eight major brain cell types, excitatory neurons (Exc) had the highest expression of *CYP1B1* (**Figure 9 (a**)). Finally, eQTL analysis of cell type specific *CYP1B1* expression in excitatory neurons showed that the rs2113389 T-allele was associated with higher cell type-specific *CYP1B1* expression levels (*p*-value= 0.035; **Figure 9 (b**)).

Blood-based DNA methylation QTLs of rs2113389

The DNA methylation QTL analysis (meQTL) of rs2113389 with CpGs in *CYP1B1* measured in blood identified three CpGs located in the *CYP1B1* gene body region associated with rs2113389 (*p*-value < 1 x 10^{-5}; **Figure 10**). The rs2113389 T-allele was associated with higher CpG expression levels.

Cyp1b1 expression and expression changes in the brain of AD mice

Cyp1b1 expression was increased in the cortex of 6-month-old hTAU mice, consistent with our findings in humans (*p*-value=0.038; **Figure 11 (a)**). *Cyp1b1* expression also significantly changed with time (genotype*age) in rTg4510 mice (FDR corrected *p*-value=0.040) but not J20 mice relative to wild-type mice (**Figure 11 (b)** and **Figure 11 (c**)). *Cyp1b1* differential expression over time in the TG rTg4510 mice was associated with entorhinal cortex tau pathology (FDR-corrected *p*-value=0.002; **Figure 11b** and **Figure 11c**).

Discussion

We performed a genome-wide association analysis (GWAS) of cortical tau PET and identified and replicated a novel SNP at the *CYP1B1-RMDN2* locus at 2p22.2. The most significant SNP at the locus originated from rs2113389, with the minor allele (T) of rs2113389 associated with higher MTL and cortical tau. Higher tau levels in rs2113389 T-allele carriers were observed across diagnoses. An additive effect of the T-allele with *APOE4* status was also observed, with minor T-allele carriers and *APOE*4 carriers having the highest tau levels. Similar findings were seen with Aβ positivity, such that Aβ+ carriers of the rs2113389 T-allele had the highest tau level. In sex-stratified analyses, generally similar results were observed, except for an interaction of Aβ positivity and rs2113389 genotype on MTL tau in females. Overall, these results provide converging evidence that the minor allele (T) of rs2113389 is a risk variant for high tau. Voxel-wise whole brain analysis confirmed that the rs2113389 T-allele was associated with tau in AD-related cortical regions. These findings also support a previous GWAS of CSF tau, where rs1478361, which is in strong LD with rs2113389 (r^2 = 0.96 and D' = 1.00), was associated with CSF total tau levels (n=3,076; β=0.0176; *p*-value=0.0295).[14]

The two protein coding genes at the locus identified in this analysis (*CYP1B1* and *RMDN2*) are highly expressed in the brain. *RMDN2* (Regulator of Microtubule Dynamics 2) is down-regulated in the parahippocampal gyrus in AD, while *CYP1B1* (Cytochrome P450 Family 1 Subfamily B Member 1) is up-regulated in the temporal cortex in AD. The minor allele of rs2113389 is also associated with higher temporal cortex *CYP1B1* expression levels. Fibroblasts and excitatory neurons had the highest expression levels of the *CYP1B1* gene in the brain, and in excitatory neurons, the minor allele of rs2113389 was associated with higher expression levels of the *CYP1B1*

gene. Blood-based DNA methylation analysis also supported the impact of the rs2113389 on CpGs within the *CYP1B1* gene, with the minor allele of rs2113389 associated with higher CpG expression. Finally, *Cyp1b1* expression was higher in the cortex of 6-month-old hTAU mice relative to controls. In addition, in the longitudinal analysis, *Cyp1b1* expression changed with aging in rTg4510 mice but not J20 mice, which suggests that *Cyp1b1* expression was associated with progression of tau but not amyloid pathology.

CYP1B1 is of particular interest as the eQTL analysis shows altered temporal lobe expression in AD patients, and rs2113389 genotype is linked to the amount of temporal lobe *CYP1B1* expression. *CYP1B1* is a member of the cytochrome p450 enzyme family (CYP). CYP is present and active in the brain and expressed in a region- and cell-specific manner, including in the blood-brain barrier.[50-52] CYP is responsible for oxidative metabolism of exogenous and endogenous substrates, potentially having both neuroprotective and pathologic roles.[51] CYP is also involved in modulating blood flow, metabolism of fatty acids, cholesterol, and neurotransmitters, and mobilization of intracellular calcium,[53-56] suggesting multiple potential roles in AD. Previously, genetic variants in CYP genes have been associated with neurodegenerative diseases, including AD,[57,58] as well as AD pathophysiology (Aβ and tau).[53,59-61] *CYP1B1* regulates endogenous pathways involved in metabolism of drugs and synthesis of cholesterols, steroids, and other lipids.[62] While several cytochrome P450 family genes such as *CYP2C19* have been implicated in AD, *CYP1B1* has not previously been directly implicated in AD.[57,58,61] However, *CYP1B1* may have multiple potential roles related to AD-related tau pathology and has been shown to be a regulator of oxidative stress, which in turn promotes angiogenesis.[63,64] *CYP1B1* also promotes angiogenesis by suppressing NF-kB activity, which is also implicated in inflammation.[65] Previous studies suggested that *CYP1B1* inhibition reduced oxidative stress and metabolized cell products

that modulate intracellular oxidative stress; however, a lack of *CYP1B1* leads to increased intracellular oxidative stress in the endothelium.[66-68] *CYP1B1* may play an important role in high fat diet-associated learning and memory deficits and oxidative damage.[68] Increased brain oxidative stress causes damage to cell function with aging and is an important pathogenic factor in AD, contributing to tau phosphorylation and the formation of neurofibrillary tangles.[69-71] Functional studies for *RMDN2* are limited, only showing that it encodes a protein important for regulating microtubule dynamics.

Pathway-based analysis identified enrichment in pathways related to the MHC, postsynaptic membrane, postsynaptic density, synapse organization, and calcium channel activity. MHC proteins and signaling have been implicated in large-scale AD genetic associations,[4,72,73] along with associations with specific MHC alleles.[74] Microglial activation via MHC class II signaling is increased in regions of phosphorylated tau.[75] Dysfunctional synaptic connections are involved early in AD-related cognitive impairment,[76] and tau deposition may induce synaptic impairment and learning deficits.[77,78] Studies also suggest a role for tau at dendritic spines in affecting the trafficking of postsynaptic receptors.[79,80] Finally, the "Calcium Hypothesis" suggests that Ca^{2+} signaling and homeostasis are implicated in AD pathology.[81] Calcium signaling controls a variety of pathways, including activation of calpain, which has been shown to precede tau phosphorylation.[82,83] Treatments targeting calcium channels are potential pathways for novel therapeutics for neurodegenerative diseases.[83]

There are some notable limitations, as studies are primarily observational and composed only of cohorts of European ancestry. Multiethnic studies are important, and to be generalizable to other populations, our findings require replication using large community studies or international

collaborations. Although we performed the largest GWAS of tau PET to date, our meta-analysis had limited statistical power due to the moderate sample size for genetic association. Additional independent large cohorts with tau PET and GWAS data will enable validation studies.

In summary, GWAS of tau PET identified novel genetic variants in a locus (*CYP1B1-RMDN2*) that influences MTL and cortical tau. The mechanistic significance of this locus was supported by a range of independent functional genomic observations in humans and model systems. Taken together, these results can inform future biomarker and therapeutic development.

Acknowledgements

Data collection and sharing for this project was funded by the Alzheimer's Disease Neuroimaging Initiative (ADNI) (National Institutes of Health Grant U01AG024904) and DOD ADNI (Department of Defense award number W81XWH-12-2-0012). ADNI is funded by the National Institute on Aging, the National Institute of Biomedical Imaging and Bioengineering, and through generous contributions from the following: AbbVie, Alzheimer's Association; Alzheimer's Drug Discovery Foundation; Araclon Biotech; BioClinica, Inc.; Biogen; Bristol-Myers Squibb Company; CereSpir, Inc.; Cogstate; Eisai Inc.; Elan Pharmaceuticals, Inc.; Eli Lilly and Company; EuroImmun; F. Hoffmann-La Roche Ltd and its affiliated company Genentech, Inc.; Fujirebio; GE Healthcare; IXICO Ltd.; Janssen Alzheimer Immunotherapy Research & Development, LLC.; Johnson & Johnson Pharmaceutical Research & Development LLC.; Lumosity; Lundbeck; Merck & Co., Inc.; Meso Scale Diagnostics, LLC.; NeuroRx Research; Neurotrack Technologies; Novartis Pharmaceuticals Corporation; Pfizer Inc.; Piramal Imaging; Servier; Takeda Pharmaceutical Company; and Transition Therapeutics. The Canadian Institutes of Health Research is providing funds to support ADNI clinical sites in Canada. Private sector contributions

are facilitated by the Foundation for the National Institutes of Health (http://www.fnih.org). The grantee organization is the Northern California Institute for Research and Education, and the study is coordinated by the Alzheimer's Therapeutic Research Institute at the University of Southern California. ADNI data are disseminated by the Laboratory for Neuro Imaging at the University of Southern California. AVID Radiopharmaceuticals, Inc., supplied the AV-1451 precursor, chemistry production advice and oversight; the FDA provided regulatory cross-filing permission and documentation needed for work in the MCSA cohort.

Funding

Data collection and sharing for this project was funded by the Alzheimer's Disease Neuroimaging Initiative (ADNI) (National Institutes of Health Grant U19 AG024904) and DOD ADNI (Department of Defense award number W81XWH-12-2-0012). Additional support for data collection and/or analysis was provided by R01 LM012535, R03 AG054936, P30 AG010133, P30 AG072976, R01 AG019771, R01 AG057739, R01 LM013463, R01 AG068193, U01 AG068057, U01 AG072177, R01 LM011360, DOD W81XWH-14-2-0151, NIGMS P50GM115318, NCATS UL1 TR001108, K01 AG049050, R01 AG061788, R01 AG052446, R01 AG052521, RF1 AG052525, P30 AG066468, P01 AG025204, and Donor's Cure Foundation. The AIBL study has received partial financial support from the Alzheimer's Association (US), the Alzheimer's Drug Discovery Foundation, an Anonymous foundation (a philanthropic foundation based in the US; one of the conditions of the funding is maintenance of anonymity), the Science and Industry Endowment Fund, the Dementia Collaborative Research Centres, the Victorian Government's Operational Infrastructure Support program, the Australian Alzheimer's Research Foundation, the National Health and Medical Research Council (NHMRC) Australia, and The Yulgilbar

Foundation. Numerous commercial interactions have supported data collection and analyses. In-kind support has also been provided by Sir Charles Gairdner Hospital, Cogstate Ltd., Hollywood Private Hospital, The University of Melbourne, and St Vincent's Hospital. Additional support for data collection and/or analysis was provided by NHMRC grants (GNT1161706, GNT1191535) awarded to SML. Support for the Harvard Aging Brain Study (HABS) was provided by NIH-NIA Program Project P01-AG036694. NIH-NIA K23AG062750. The A4 study was funded by the National Institute on Aging (grants U19AG010483 and R01AG063689, Eli Lilly and Co, and several philanthropic organizations (NCT02008357). The Mayo Clinic Study of Aging (MCSA) funding includes NIH grants U01 AG006786, R01 NS097495, R01 AG56366, P50 AG016574, P30 AG062677, R37 AG011378, R01 AG041851, R01 AG034676, C06 RR018898. The GHR Foundation, the Alexander Family Alzheimer's Disease Research Professorship of the Mayo Clinic, the Alzheimer's Association, the Mayo Foundation for Medical Education and Research, the Liston Award, the Elsie and Marvin Dekelboum Family Foundation, the Schuler Foundation. National Centralized Repository for Alzheimer's Disease and Related Dementias (NCRAD): U24AG021886. This work was supported by grants from the National Institutes of Health, R01AG044546, P01AG003991, RF1AG053303, RF1AG058501, U01AG058922, and the Chan Zuckerberg Initiative (CZI), the Michael J. Fox Foundation, the Department of Defense (LI-W81XWH2010849) and the Alzheimer's Association Zenith Fellows Award (ZEN-22-848604). The recruitment and clinical characterization of research participants at Washington University were supported by NIH P30AG066444, P01AG03991, and P01AG026276. This work was supported by access to equipment made possible by the Hope Center for Neurological Disorders, the Neurogenomics and Informatics Center (NGI: https://neurogenomics.wustl.edu/) and the Departments of Neurology and Psychiatry at Washington University School of Medicine.

Additional funding from NIH National Institute on Aging includes R01 AG059716, R01 AG061518, R01 AG034570, and P30 AG066468. The University of Pittsburgh School of Public Health, Department of Genetics includes R01 AG064877 and P30 AG066468. California-Lawrence Berkeley National Laboratory includes R01 AG034570 and R01 AG062542. The rTg4510 and J20 mouse work was funded in part through the Medical Research Council (MRC) Proximity to Discovery: Industry Engagement Fund (Precision Medicine Exeter Innovation Platform reference MC_PC_14127), an MRC Clinical Infrastructure award (MR/M008924/1), a Wellcome Trust Multi-User Equipment Award (WT101650MA) and through a research grant from Alzheimer's Research UK (ARUK-PG2018B-016).

Declaration of interests

Dr. Apostolova received grant or other financial support from the National Institutes of Health (NIH), Alzheimer's Association, AVID Pharmaceuticals, Life Molecular Imaging, Roche Diagnostics, and Eli Lilly. In addition, she has received consulting fees from Biogen, Two Labs, IQIVA, Florida Department of Health, Genentech, NIH Biobank, Eli Lilly, GE Healthcare, Eisai, and Roche Diagnostics. She has also received payment or honoraria from American Academy of Neurology, MillerMed, National Alzheimer's Coordinating Center CME, CME Institute, APhA, Purdue University, Mayo Clinic, MJH Physician Education Resource, and Ohio State University. She received support for travel from the Alzheimer's Association. She has served on Data Safety and Monitoring or Advisory Boards for IQVIA, UAB Nathan Schock Center, New Mexico Exploratory ADRC, and NIA R01 AG061111. She has a leadership role in multiple committees, including the Medical Science Council of the Alzheimer's Association Greater Indiana Chapter, the Alzheimer's Association Science Program Committee, and the FDA PCNS Advisory Committee. Finally, Dr. Apostolova holds stock in Cassava Neurosciences and Golden Seeds.

Dr. Foroud receives support from multiple NIH grants (U24 NS095871, U24 AG021886, U24 AG056270, U01 AA026103, U10 AA008401, P30 AG010133, R01 AG019771, U01 AG032984, P30 AR072581, U01 AG057195, UL1 TR002529, U19 AG063911; U19 AG063744, U19 AG068054, R01 AG069453, U54 CA196519, R01 AG061146, R01 AG073267, R01 AG074971, U19 AG071754, R01 AG055444, R01 AG070349, U19 AG024904, R01 AG076634, U19 AG079774, U54 CA280897, U19 NS120384); the Michael J. Fox Foundation (MJFF001948); Cohen Veterans Biosciences; The Parkinson's Disease Foundation; Children's Tumor Foundation; Broad Institute; Lumind Foundation; and Gates Venture (0432-06-120975).

Dr. Jagust has served as a consultant for Biogen, Eisai, Lilly, and Bioclinica. He has an equity interest in Optoceuticals.

Aparna Vasanthakumar and Jeffrey F. Waring are employees of AbbVie and may own AbbVie stock.

Dr. Hohman receives support from multiple NIH grants (U24-AG074855, P20-AG068082, R01-AG061518, R01-AG059716, R01-AG074012, RF1-AG059869). He also sits on the advisory board for Vivid Genomics and is a Senior Associate Editor for Alzheimer's and Dementia: Translational Research and Clinical Intervention.

Hyun-Sik Yang received personal fees (honorarium) from Genentech, Inc outside the submitted work.

Dr. Vemuri receives funding support from the NIH.

Dr. Cruchaga has received research support from: GSK and EISAI. The funders of the study had no role in the collection, analysis, or interpretation of data; in the writing of the report; or in the

decision to submit the paper for publication. Dr. Cruchaga is a member of the advisory board of Vivid Genomics and Circular Genomics.

Dr. Saykin receives support from multiple NIH grants (P30 AG010133, P30 AG072976, R01 AG019771, R01 AG057739, U19 AG024904, R01 LM013463, R01 AG068193, T32 AG071444, and U01 AG068057 and U01 AG072177). He has also received support from Avid Radiopharmaceuticals, a subsidiary of Eli Lilly (in kind contribution of PET tracer precursor); Bayer Oncology (Scientific Advisory Board); Eisai (Scientific Advisory Board); Siemens Medical Solutions USA, Inc. (Dementia Advisory Board); NIH NHLBI (MESA Observational Study Monitoring Board); Springer-Nature Publishing (Editorial Office Support as Editor-in-Chief, Brain Imaging and Behavior).

The other authors declare no conflict of interest.

Author Contributions

KN, SLR, and AJS were involved with study design, statistical analysis, data generation, and drafting of the final manuscript.

PJB was involved with drafting of the final manuscript.

LGA, JB, MRF, TF, KN, PA, RS, BH, SS, DS, CRJ, WJJ, SL, AV, JFW, VD, SML, TP, CCR, VLV, LD, TJH, JL, EM, RFB, KJ, HSY, RCP, VKR, PV, ADC, KHF, MIK, OLL, DAB, MA, TB, CC, DH, PLDJ, MF, VJ, BTL, APT, IC, JM, and MWW were all involved with generation of the imaging, genetic, other "omics," and/or animal model data.

RD, KF, TYJ, JPK, KN, BH, AV, VD, VLV, SML, TP, LD, TJH, JL, EM, RFB, HSY, ADC, KHF, DAB, VJ, APT, and IC were involved with processing and analysis of imaging and "omics" data.

All authors reviewed and approved the final submitted manuscript.

Figures

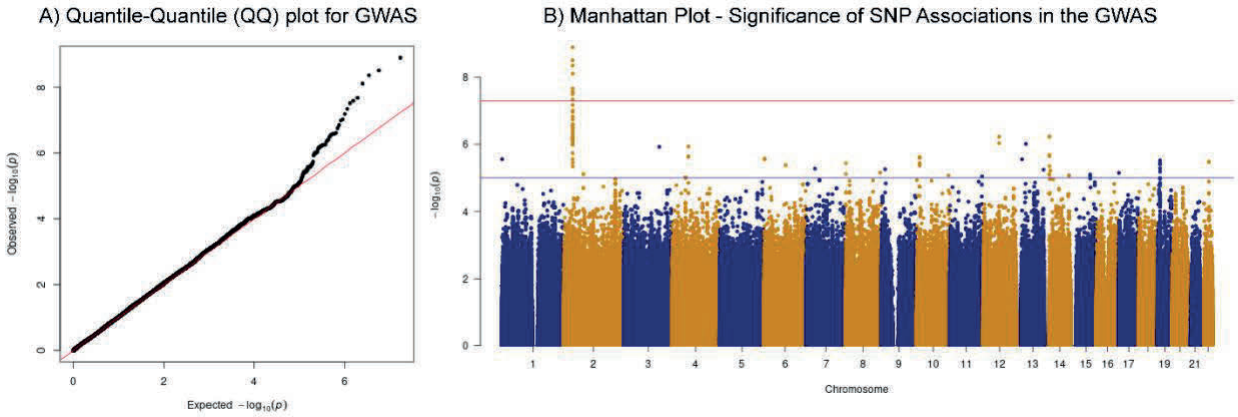

Figure 1. Results of Discovery GWAS for cortical tau deposition

Quantile-quantile (QQ) (A) and Manhattan (B) plots of genome-wide association study (GWAS) results are shown. The genomic inflation factor is λ=1.025 In the Manhattan plot, the horizontal blue and red lines represent the $-\log_{10}(10^{-5})$ and $-\log_{10}(5.0 \times 10^{-8})$ threshold levels, respectively. Two single nucleotide polymorphisms (SNPs) on chromosome 2 showed highly significant ($<5.0 \times 10^{-8}$) associations with cerebral tau deposition. *Note: cerebral tau endophenotype measured as an inverse normal transformed variable of cortical tau SUVR.*

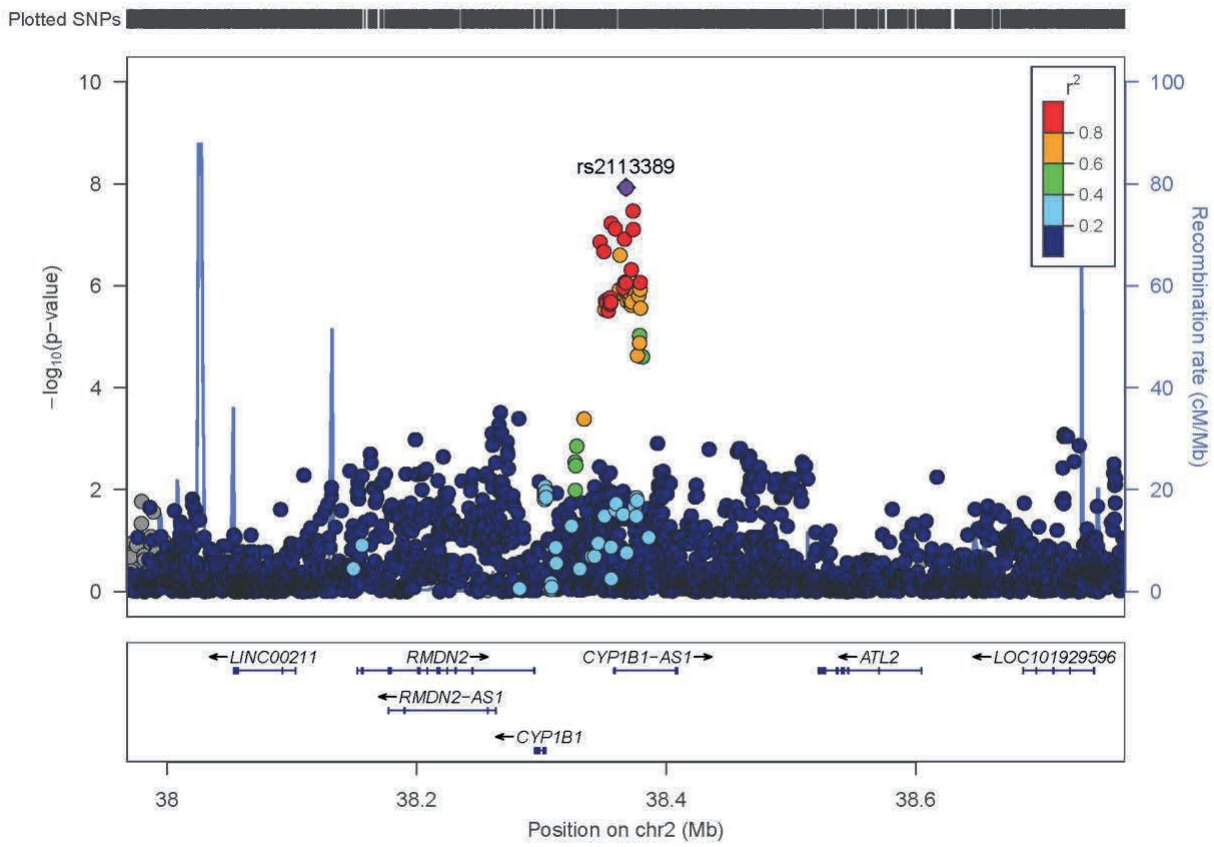

Figure 2. LocusZoom plot of most strongly associated SNPs in the locus (*RMDN2-CYP1B1*)

The regional association plot for the locus that passed genome-wide significance shows the region around the most significant SNP (rs2113389) at the *RMDN2-CYP1B1* locus. SNPs were plotted based on their GWAS $-\log_{10}$ *p*-values and genomic position. The red color scale of r^2 values was used to label SNPs based on their degree of linkage disequilibrium with the most significant SNP. Recombination rates calculated from 1000 Genomes Project reference data are also displayed in a blue line corresponding to the right vertical axis.

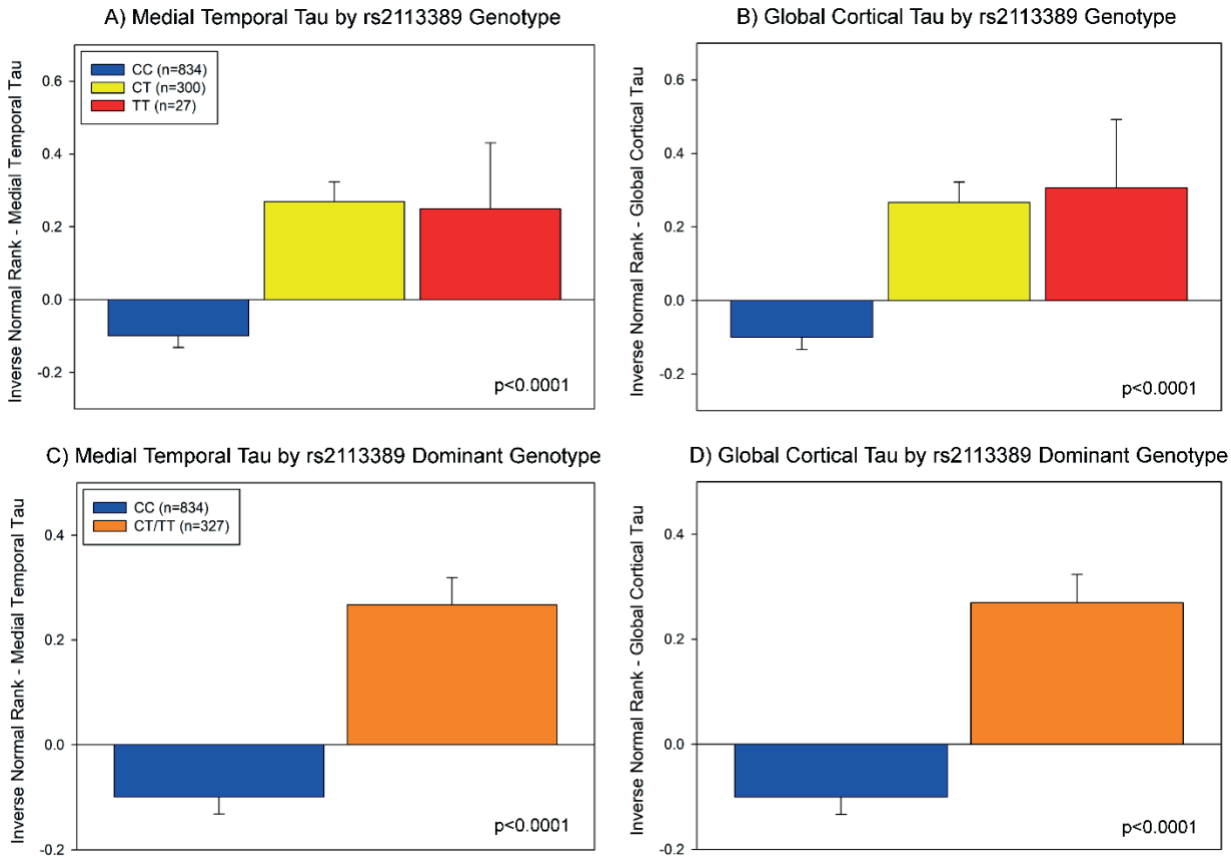

Figure 3. Association of the most significant SNP (rs2113389) at the *RMDN2-CYP1B1* locus with regional and global cortical tau burden

Using an additive model, the minor allele (T) of rs2113389 was associated with higher tau deposition across participants, with both rs2113389 CT and TT individuals showing significantly greater medial temporal lobe (A) and cortical (B) tau deposition than rs2113389 CC individuals. Similar results were seen using a dominant model. Specifically, individuals with one or more minor alleles of rs2113389 showed significantly greater tau deposition in the medial temporal lobe (C) and cortex (D) than rs2113389 CC individuals. All associations were significant at $p<0.0001$.

Note: tau measured as an inverse normal transformed variable of medial temporal and cortical tau SUVR

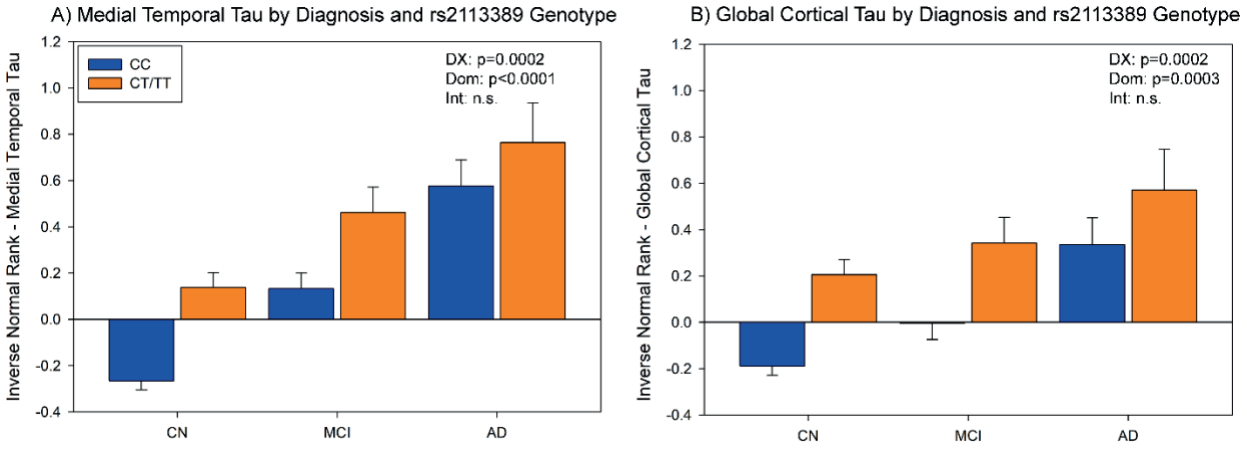

Figure 4. Interaction effect of the most significant SNP (rs2113389) at the *RMDN2-CYP1B1* locus with diagnosis on regional and cortical tau deposition

Both diagnosis and rs2113389 dominant genotype were significantly associated with medial temporal (A) and cortical (B) tau deposition (all $p<0.001$), such that AD participants who carry at least one minor allele (T) of rs2113389 have the highest tau level relative to all other diagnoses and CC rs2113389 individuals. AD=Alzheimer's disease; CN=cognitively normal; DX=diagnosis; Dom=rs2113389 dominant genotype (CC vs. CT/TT); Int.=interaction; MCI=mild cognitive impairment; n.s.=not significant; *Note: tau measured as an inverse normal transformed variable of medial temporal and cortical tau SUVR*

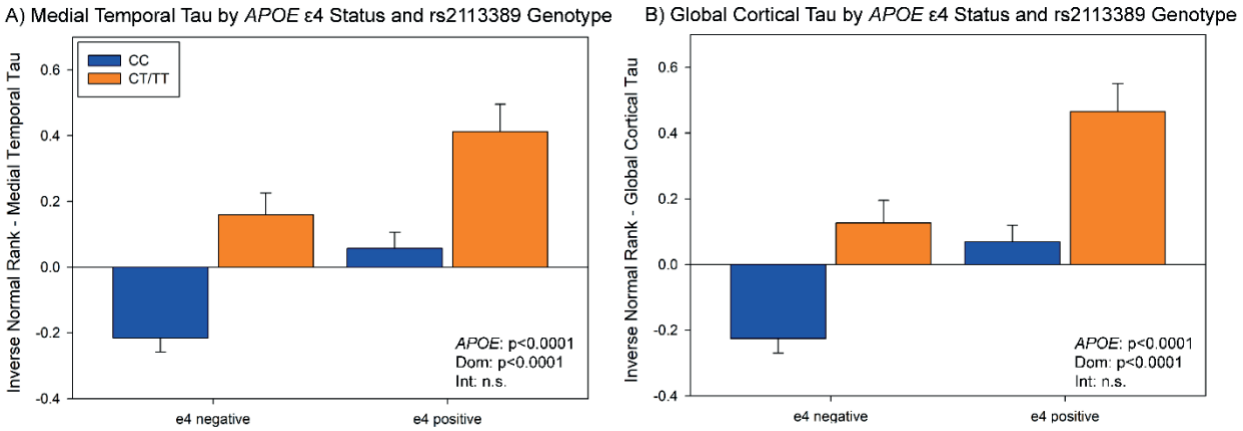

Figure 5. Interaction effect of the most significant SNP (rs2113389) at the *RMDN2-CYP1B1* locus with *APOE4* carrier status on regional and cortical tau deposition

APOE4 carrier status and rs2113389 dominant genotype are significantly associated with medial temporal (A) and cortical (B) tau deposition (all p<0.0001). The highest tau level is observed in carriers of both at least one *APOE4* allele and minor allele (T) at rs2113389, relative to either CC rs2113389 individuals or *APOE4* negative individuals. APOE=apolipoprotein E; Dom=rs2113389 dominant genotype (CC vs. CT/TT); Int.=interaction; MCI=mild cognitive impairment; n.s.=not significant; *Note: tau measured as an inverse normal transformed variable of medial temporal and cortical tau SUVR*

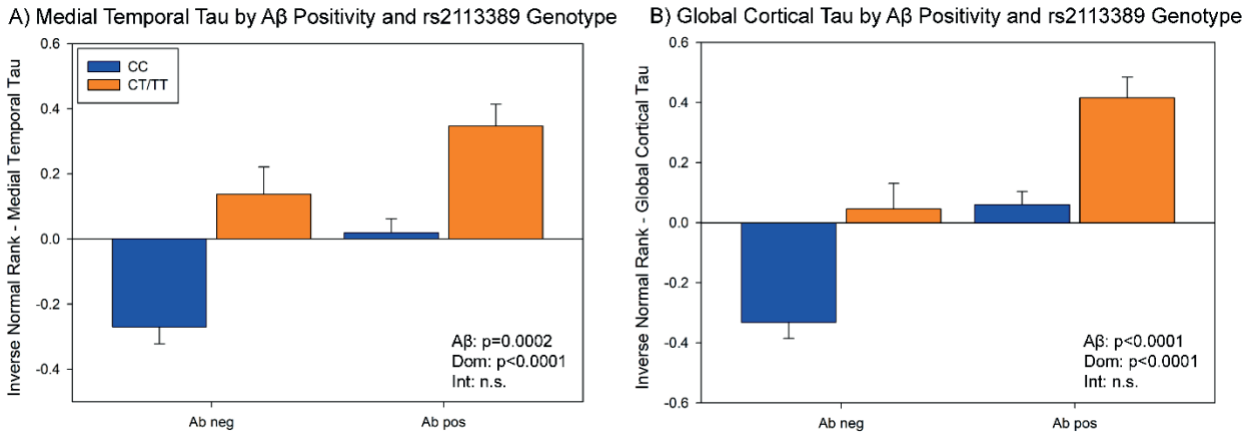

Figure 6. Interaction effect of the most significant SNP (rs2113389) at the *RMDN2-CYP1B1* locus with Aβ positivity on regional and cortical tau deposition

Significant effects of both Aβ positivity and rs2113389 dominant genotype on medial temporal (A) and cortical (B) tau deposition are observed (all $p<0.001$), with Aβ positive individuals carrying at least one minor allele (T) at rs2113389 showing the highest level of tau deposition relative to all other groups (Aβ negative individuals, rs2113389 CC individuals). Aβ=amyloid-beta; Dom=rs2113389 dominant genotype (CC vs. CT/TT); Int.=interaction; MCI=mild cognitive impairment; n.s.=not significant; *Note: tau measured as an inverse normal transformed variable of medial temporal and cortical tau SUVR*

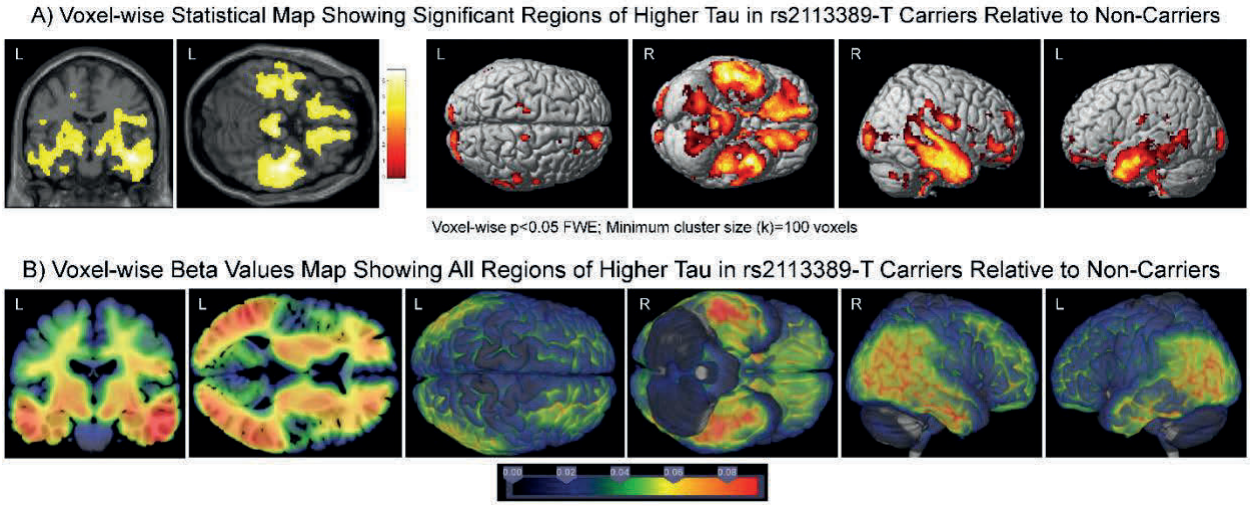

Figure 7. Voxel-wise analysis and visualization of the effect of rs2113389 dominant genotype on tau deposition

(A) Widespread regions of association between rs2113389 dominant genotype and tau deposition are observed in the inferior frontal, parietal, and medial and lateral temporal lobes, such that those with one or more minor alleles (T) at rs2113389 show greater tau deposition than CC rs2113389 individuals. Images are displayed at a voxel-wise threshold of $p<0.05$ with family-wise error correction for multiple comparisons and a minimum cluster size (k)=100 voxels. (B) Beta-value maps show widespread regions of higher tau deposition in rs2113389-T carriers relative to non-carriers. Specifically, temporal, parietal, and frontal lobe tau is greater in minor allele carriers than non-carriers.

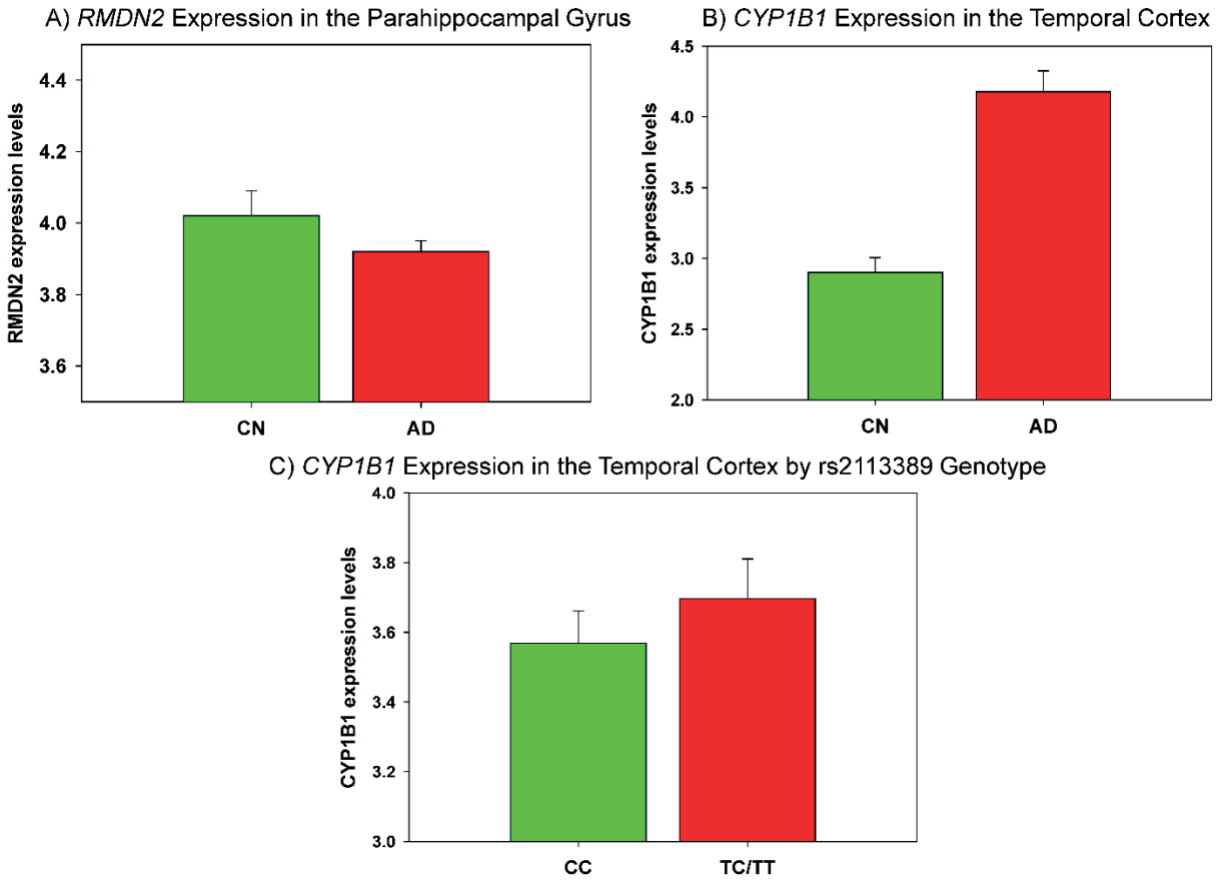

Figure 8. Gene expression of *RMDN2* and *CYP1B1* by diagnosis and rs2113389 dominant genotype

Patients with AD showed downregulated expression of *RMDN2* in the parahippocampal gyri (A) and upregulated expression of *CYP1B1* in the temporal cortex (B) relative to CN individuals using brain tissue-based RNA-Seq data from the AMP-AD project. (C) In an eQTL analysis, the identified SNP (rs2113389) was shown to be associated with *CYP1B1* expression levels in the temporal cortex, with carriers of the minor allele showing upregulated *CYP1B1* expression relative to individuals with the rs2113389 CC genotype. AD=Alzheimer's disease; CN=cognitively normal

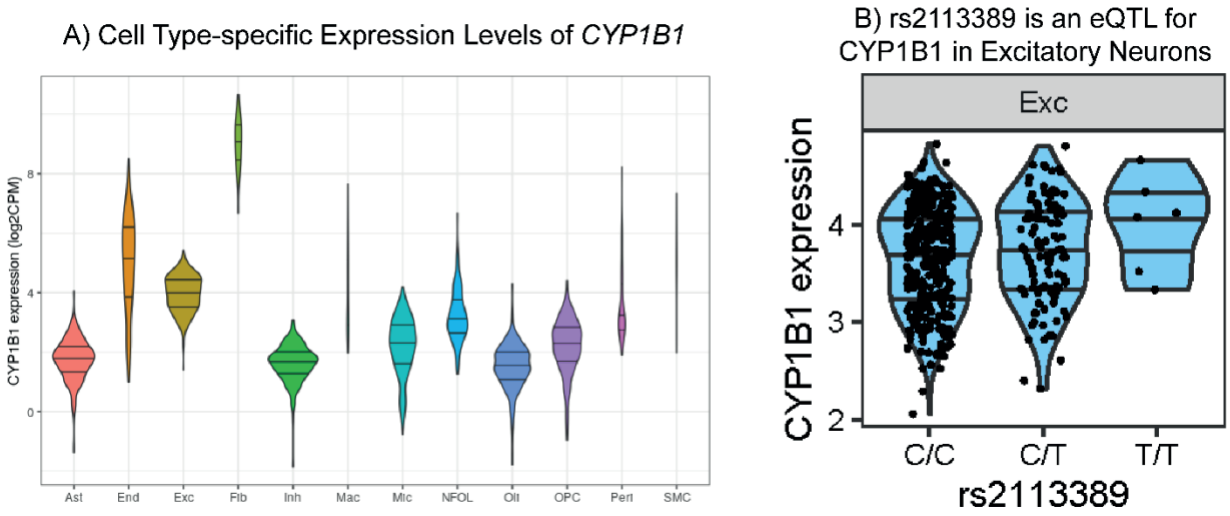

Figure 9. Cell type-specific expression and eQTL of *CYP1B1*

Cell type-specific expression levels (A) and eQTL in the excitatory neuron (B) of *CYP1B1* gene are shown. In (A), the x-axis is cell types in ROSMAP DLPFC single-nucleus RNA-Seq data. The y-axis is the $\log_2$ of counts per million mapped reads (CPM) of *CYP1B1* gene. Bars show the 25%, 50%, and 75% quartiles, respectively. Expression levels were computed at the donor level, by aggregating cells from the same donor. Rare cell types were observed only in a small fraction of donors. To reflect this, areas of violin plots are scaled proportionally to the number of donors. Fibroblasts (Fib) had the highest expression of *CYP1B1* gene. Among major cell types, excitatory neurons (Exc) had the highest expression. In (B), the minor allele (T) of rs2113389 was associated with higher cell type-specific *CYP1B1* expression levels in the excitatory neuron (p-value= 0.035).

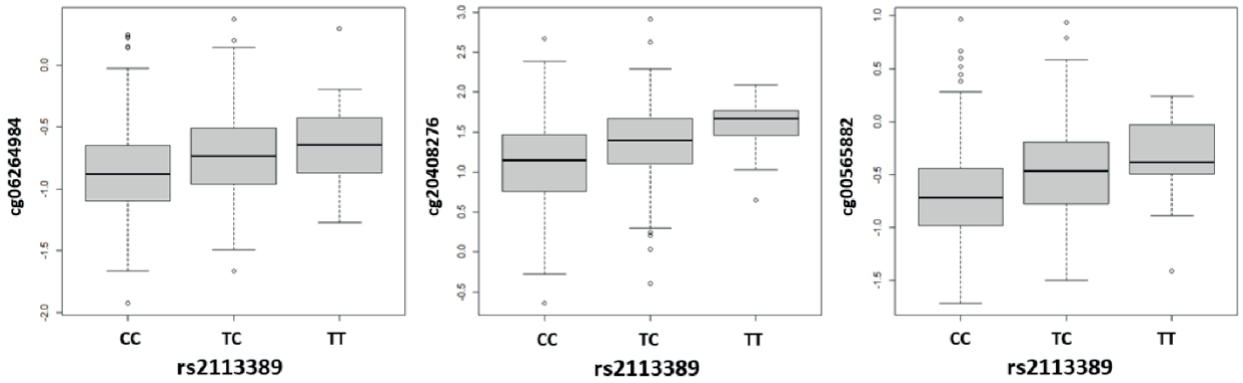

Figure 10. Blood-based DNA methylation QTLs of rs211338

DNA methylation QTL analysis (*cis*-meQTL) of rs2113389 with CpGs in *CYP1B1* measured in blood samples from 634 ADNI participants identified three CpGs, located in the *CYP1B1* gene body region, as significantly associated with rs2113389 (p-value < 1 x 10^{-5}). The minor allele (T) of rs2113389 was associated with higher expression levels of the CpGs.

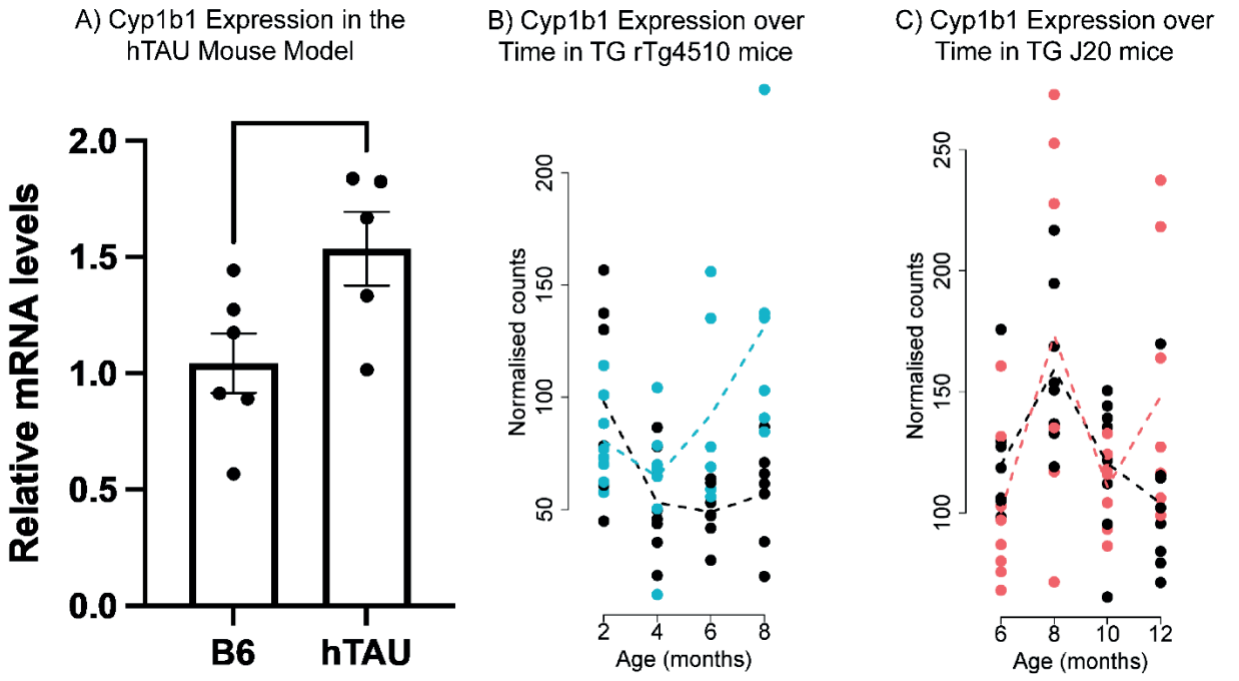

Figure 11. *Cyp1b1* expression and expression changes in the brain of tau (hTAU, rTg4510) and amyloid (J20) mice

(A) *Cyp1b1* expression was increased in the hTAU mouse model expressing six isoforms of human tau, consistent with our findings in human LOAD (*p*-value=0.038). In hTAU mice, *Cyp1b1* expression was increased in the cortex of 6-month-old mice. (B) *Cyp1b1* expression significantly changed with time (genotype*age) in TG rTg4510 mice, i.e., *Cyp1b1* is associated with disease progression in the rTg4510 model. *Cyb1b1* is also specifically associated with tau pathology progression. (C) *Cyp1b1* expression did not change with time (genotype*age) in J20 mice, i.e., *Cyp1b1* is not associated with disease progression in the J20 model. In addition, *Cyb1b1* is not associated with amyloid pathology progression.

Table 1. List of top gene ontology (GO) pathways for global cortical tau deposition.

Pathway maps	**Set size**[a]	**z-score**	**q-value**
Homophilic cell adhesion via plasma membrane adhesion molecules	151(154)	6.24	1.38E-6
Regulation of Ras protein signal transduction	182(192)	6.06	2.22E-6
Ras guanyl-nucleotide exchange factor activity	123(130)	5.97	2.51E-6
Guanyl-nucleotide exchange factor activity	192(205)	5.93	2.51E-6
Plasma membrane organization	197(199)	5.80	4.46E-6
UDP-glycosyltransferase activity	128(139)	5.21	1.04E-4
Interaction with host	157(159)	5.12	1.44E-4
Flavonoid glucuronidation	21(21)	5.06	1.71E-4
Protein autophosphorylation	179(189)	5.04	1.71E-4
Regulation of Rho protein signal transduction	105(110)	5.03	1.71E-4
Positive regulation of leukocyte cell-cell adhesion	192(208)	4.99	1.81E-4
Positive regulation of homotypic cell-cell adhesion	191(207)	4.97	1.81E-4
Positive regulation of T cell activation	187(203)	4.93	2.06E-4
Protein tyrosine kinase activity	140(146)	4.84	3.00E-4
Cellular glucuronidation	25(25)	4.83	3.00E-4
Antigen binding	81(234)	4.80	3.24E-4
Calcium ion transmembrane transport	132(136)	4.67	5.69E-4
Glucuronosyltransferase activity	33(34)	4.67	5.69E-4
Divalent inorganic cation transmembrane transporter activity	155(162)	4.64	5.94E-4
Phosphatidylinositol binding	187(195)	4.64	5.94E-4
Lamellipodium	163(169)	4.58	7.18E-4
Flavonoid biosynthetic process	19(19)	4.57	7.28E-4

Set size[a]: Number of genes from study data (number of genes in the pathway).

Table 2. List of top the Kyoto Encyclopedia of genes and genomes (KEGG) pathways for global cortical tau deposition level.

Pathway maps	**Set size**[a]	**z-score**	**q-value**
Focal adhesion	194(202)	4.74	2.01E-4
Cell adhesion molecules (CAMs)	127(137)	4.71	2.01E-4
Ascorbate and aldarate metabolism	26(27)	4.51	2.02E-4
Type I diabetes mellitus	43(47)	4.24	5.23E-4
Viral myocarditis	69(76)	4.17	5.86E-4
Endocytosis	195(206)	4.09	6.72E-4
Phagosome	144(160)	4.06	6.72E-4
Allograft rejection	36(41)	4.02	6.97E-4
Bacterial invasion of epithelial cells	69(74)	3.82	1.43E-3
Porphyrin and chlorophyll metabolism	41(44)	3.72	1.88E-3
Pentose and glucuronate interconversions	29(30)	3.66	2.17E-3
ECM-receptor interaction	84(85)	3.53	3.27E-3
Calcium signaling pathway	168(179)	3.34	6.08E-3
Autoimmune thyroid disease	51(56)	3.33	6.08E-3
Renal cell carcinoma	67(71)	3.23	7.75E-3
Protein processing in endoplasmic reticulum	159(168)	3.18	8.71E-3
Type II diabetes mellitus	45(48)	3.18	8.71E-3
Steroid hormone biosynthesis	55(57)	3.16	8.71E-3
Drug metabolism - other enzymes	51(53)	3.13	8.71E-3
Complement and coagulation cascades	67(70)	3.10	9.22E-3
ABC transporters	42(45)	3.01	1.18E-2

Set size[a]: Number of genes from study data (number of genes in the pathway).

References

1. Association As. 2019 Alzheimer's Disease Facts and Figures. *Alzheimer's & Dementia* 2019; **15**(3): 321-87.

2. Jack CR, Jr., Bennett DA, Blennow K, et al. A/T/N: An unbiased descriptive classification scheme for Alzheimer disease biomarkers. *Neurology* 2016; **87**(5): 539-47.

3. Van Cauwenberghe C, Van Broeckhoven C, Sleegers K. The genetic landscape of Alzheimer disease: clinical implications and perspectives. *Genet Med* 2016; **18**(5): 421-30.

4. Kunkle BW, Grenier-Boley B, Sims R, et al. Genetic meta-analysis of diagnosed Alzheimer's disease identifies new risk loci and implicates Abeta, tau, immunity and lipid processing. *Nat Genet* 2019; **51**(3): 414-30.

5. Jansen PR, Watanabe K, Stringer S, et al. Genome-wide analysis of insomnia in 1,331,010 individuals identifies new risk loci and functional pathways. *Nat Genet* 2019; **51**(3): 394-403.

6. Liu CC, Liu CC, Kanekiyo T, Xu H, Bu G. Apolipoprotein E and Alzheimer disease: risk, mechanisms and therapy. *Nat Rev Neurol* 2013; **9**(2): 106-18.

7. Saykin AJ, Shen L, Yao X, et al. Genetic studies of quantitative MCI and AD phenotypes in ADNI: Progress, opportunities, and plans. *Alzheimers Dement* 2015; **11**(7): 792-814.

8. Li J, Zhang Q, Chen F, et al. Genetic Interactions Explain Variance in Cingulate Amyloid Burden: An AV-45 PET Genome-Wide Association and Interaction Study in the ADNI Cohort. *Biomed Res Int* 2015; **2015**: 647389.

9. Ramanan VK, Risacher SL, Nho K, et al. GWAS of longitudinal amyloid accumulation on 18F-florbetapir PET in Alzheimer's disease implicates microglial activation gene IL1RAP. *Brain : a journal of neurology* 2015; **138**(Pt 10): 3076-88.

10. Ramanan VK, Risacher SL, Nho K, et al. APOE and BCHE as modulators of cerebral amyloid deposition: a florbetapir PET genome-wide association study. *Mol Psychiatry* 2014; **19**(3): 351-7.

11. Vacher M, Porter T, Villemagne VL, et al. Validation of a priori candidate Alzheimer's disease SNPs with brain amyloid-beta deposition. *Sci Rep* 2019; **9**(1): 17069.

12. Yan Q, Nho K, Del-Aguila JL, et al. Genome-wide association study of brain amyloid deposition as measured by Pittsburgh Compound-B (PiB)-PET imaging. *Mol Psychiatry* 2021; **26**(1): 309-21.

13. Zhao QF, Wan Y, Wang HF, et al. ABCA7 Genotypes Confer Alzheimer's Disease Risk by Modulating Amyloid-beta Pathology. *J Alzheimers Dis* 2016; **52**(2): 693-703.

14. Deming Y, Li Z, Kapoor M, et al. Genome-wide association study identifies four novel loci associated with Alzheimer's endophenotypes and disease modifiers. *Acta Neuropathol* 2017; **133**(5): 839-56.

15. Franzmeier N, Rubinski A, Neitzel J, Ewers M, Alzheimer's Disease Neuroimaging I. The BIN1 rs744373 SNP is associated with increased tau-PET levels and impaired memory. *Nat Commun* 2019; **10**(1): 1766.

16. Ramanan VK, Heckman MG, Lesnick TG, et al. Tau polygenic risk scoring: a cost-effective aid for prognostic counseling in Alzheimer's disease. *Acta Neuropathol* 2022; **143**(5): 571-83.

17. Ramanan VK, Wang X, Przybelski SA, et al. Variants in PPP2R2B and IGF2BP3 are associated with higher tau deposition. *Brain Commun* 2020; **2**(2): fcaa159.

18. Komuro Y, Xu G, Bhaskar K, Lamb BT. Human tau expression reduces adult neurogenesis in a mouse model of tauopathy. *Neurobiol Aging* 2015; **36**(6): 2034-42.

19. Bemiller SM, McCray TJ, Allan K, et al. TREM2 deficiency exacerbates tau pathology through dysregulated kinase signaling in a mouse model of tauopathy. *Mol Neurodegener* 2017; **12**(1): 74.

20. Castanho I, Murray TK, Hannon E, et al. Transcriptional Signatures of Tau and Amyloid Neuropathology. *Cell Rep* 2020; **30**(6): 2040-54 e5.

21. Lee Y, Han S, Kim D, et al. Genetic variation affecting exon skipping contributes to brain structural atrophy in Alzheimer's disease. *AMIA Jt Summits Transl Sci Proc* 2018; **2017**: 124-31.

22. Kim S, Swaminathan S, Shen L, et al. Genome-wide association study of CSF biomarkers Abeta1-42, t-tau, and p-tau181p in the ADNI cohort. *Neurology* 2011; **76**(1): 69-79.

23. Price AL, Patterson NJ, Plenge RM, Weinblatt ME, Shadick NA, Reich D. Principal components analysis corrects for stratification in genome-wide association studies. *Nat Genet* 2006; **38**(8): 904-9.

24. Nho K, Corneveaux JJ, Kim S, et al. Whole-exome sequencing and imaging genetics identify functional variants for rate of change in hippocampal volume in mild cognitive impairment. *Mol Psychiatry* 2013; **18**(7): 781-7.

25. Purcell S, Neale B, Todd-Brown K, et al. PLINK: a tool set for whole-genome association and population-based linkage analyses. *Am J Hum Genet* 2007; **81**(3): 559-75.

26. Kanai M, Tanaka T, Okada Y. Empirical estimation of genome-wide significance thresholds based on the 1000 Genomes Project data set. *J Hum Genet* 2016; **61**(10): 861-6.

27. Pruim RJ, Welch RP, Sanna S, et al. LocusZoom: regional visualization of genome-wide association scan results. *Bioinformatics* 2010; **26**(18): 2336-7.

28. Yoon S, Nguyen HCT, Yoo YJ, et al. Efficient pathway enrichment and network analysis of GWAS summary data using GSA-SNP2. *Nucleic Acids Res* 2018; **46**(10): e60.

29. Horgusluoglu-Moloch E, Risacher SL, Crane PK, et al. Genome-wide association analysis of hippocampal volume identifies enrichment of neurogenesis-related pathways. *Sci Rep* 2019; **9**(1): 14498.

30. Li MX, Gui HS, Kwan JS, Sham PC. GATES: a rapid and powerful gene-based association test using extended Simes procedure. *Am J Hum Genet* 2011; **88**(3): 283-93.

31. Allen M, Carrasquillo MM, Funk C, et al. Human whole genome genotype and transcriptome data for Alzheimer's and other neurodegenerative diseases. *Sci Data* 2016; **3**: 160089.

32. De Jager PL, Ma Y, McCabe C, et al. A multi-omic atlas of the human frontal cortex for aging and Alzheimer's disease research. *Sci Data* 2018; **5**: 180142.

33. Wang M, Beckmann ND, Roussos P, et al. The Mount Sinai cohort of large-scale genomic, transcriptomic and proteomic data in Alzheimer's disease. *Sci Data* 2018; **5**: 180185.

34. Wan YW, Al-Ouran R, Mangleburg CG, et al. Meta-Analysis of the Alzheimer's Disease Human Brain Transcriptome and Functional Dissection in Mouse Models. *Cell Reports* 2020; **32**(2).

35. Logsdon BA, Perumal TM, Swarup V, et al. Meta-analysis of the human brain transcriptome identifies heterogeneity across human AD coexpression modules robust to sample collection and methodological approach. *bioRxiv* 2019: 510420.

36. Võsa U, Claringbould A, Westra HJ, et al. Large-scale cis- and trans-eQTL analyses identify thousands of genetic loci and polygenic scores that regulate blood gene expression. *Nat Genet* 2021; **53**(9): 1300-10.

37. Bennett DA, Buchman AS, Boyle PA, Barnes LL, Wilson RS, Schneider JA. Religious Orders Study and Rush Memory and Aging Project. *J Alzheimers Dis* 2018; **64**(s1): S161-S89.

38. Vasanthakumar A, Davis JW, Idler K, et al. Harnessing peripheral DNA methylation differences in the Alzheimer's Disease Neuroimaging Initiative (ADNI) to reveal novel biomarkers of disease. *Clin Epigenetics* 2020; **12**(1): 84.

39. Kim JP, Kim BH, Bice PJ, et al. Integrative Co-methylation Network Analysis Identifies Novel DNA Methylation Signatures and Their Target Genes in Alzheimer's Disease. *Biol Psychiatry* 2022.

40. Li QS, Vasanthakumar A, Davis JW, et al. Association of peripheral blood DNA methylation level with Alzheimer's disease progression. *Clin Epigenetics* 2021; **13**(1): 191.

41. Jadhav VS, Lin PBC, Pennington T, et al. Trem2 Y38C mutation and loss of Trem2 impairs neuronal synapses in adult mice. *Molecular Neurodegeneration* 2020; **15**(1): 62.

42. Tsai AP, Dong C, Lin PB-C, et al. PLCG2 is associated with the inflammatory response and is induced by amyloid plaques in Alzheimer's disease. *Genome Medicine* 2022; **14**(1): 17.

43. Ramsden M, Kotilinek L, Forster C, et al. Age-dependent neurofibrillary tangle formation, neuron loss, and memory impairment in a mouse model of human tauopathy (P301L). *J Neurosci* 2005; **25**(46): 10637-47.

44. Santacruz K, Lewis J, Spires T, et al. Tau suppression in a neurodegenerative mouse model improves memory function. *Science* 2005; **309**(5733): 476-81.

45. Hsia AY, Masliah E, McConlogue L, et al. Plaque-independent disruption of neural circuits in Alzheimer's disease mouse models. *Proc Natl Acad Sci U S A* 1999; **96**(6): 3228-33.

46. Mucke L, Masliah E, Yu GQ, et al. High-level neuronal expression of abeta 1-42 in wild-type human amyloid protein precursor transgenic mice: synaptotoxicity without plaque formation. *J Neurosci* 2000; **20**(11): 4050-8.

47. Love MI, Huber W, Anders S. Moderated estimation of fold change and dispersion for RNA-seq data with DESeq2. *Genome Biol* 2014; **15**(12): 550.

48. Benjamini Y, Hochberg Y. Controlling the False Discovery Rate - a Practical and Powerful Approach to Multiple Testing. *J R Stat Soc B* 1995; **57**(1): 289-300.

49. Yang J, Lee SH, Goddard ME, Visscher PM. GCTA: a tool for genome-wide complex trait analysis. *Am J Hum Genet* 2011; **88**(1): 76-82.

50. Ferguson CS, Tyndale RF. Cytochrome P450 enzymes in the brain: emerging evidence of biological significance. *Trends Pharmacol Sci* 2011; **32**(12): 708-14.

51. Ghosh C, Hossain M, Solanki J, Dadas A, Marchi N, Janigro D. Pathophysiological implications of neurovascular P450 in brain disorders. *Drug Discov Today* 2016; **21**(10): 1609-19.

52. Ghosh C, Gonzalez-Martinez J, Hossain M, et al. Pattern of P450 expression at the human blood-brain barrier: roles of epileptic condition and laminar flow. *Epilepsia* 2010; **51**(8): 1408-17.

53. Benedet AL, Yu L, Labbe A, et al. CYP2C19 variant mitigates Alzheimer disease pathophysiology in vivo and postmortem. *Neurol Genet* 2018; **4**(1): e216.

54. Miksys S, Tyndale RF. Cytochrome P450-mediated drug metabolism in the brain. *J Psychiatry Neurosci* 2013; **38**(3): 152-63.

55. Iliff JJ, Jia J, Nelson J, Goyagi T, Klaus J, Alkayed NJ. Epoxyeicosanoid signaling in CNS function and disease. *Prostaglandins Other Lipid Mediat* 2010; **91**(3-4): 68-84.

56. Stingl JC, Brockmoller J, Viviani R. Genetic variability of drug-metabolizing enzymes: the dual impact on psychiatric therapy and regulation of brain function. *Mol Psychiatry* 2013; **18**(3): 273-87.

57. Chace C, Pang D, Weng C, et al. Variants in CYP17 and CYP19 cytochrome P450 genes are associated with onset of Alzheimer's disease in women with down syndrome. *J Alzheimers Dis* 2012; **28**(3): 601-12.

58. Djelti F, Braudeau J, Hudry E, et al. CYP46A1 inhibition, brain cholesterol accumulation and neurodegeneration pave the way for Alzheimer's disease. *Brain : a journal of neurology* 2015; **138**(Pt 8): 2383-98.

59. Kapas I, Katko M, Harangi M, et al. Cerebrotendinous xanthomatosis with the c.379C>T (p.R127W) mutation in the CYP27A1 gene associated with premature age-associated limbic tauopathy. *Neuropathol Appl Neurobiol* 2014; **40**(3): 345-50.

60. Pappolla MA, Omar RA, Chyan YJ, et al. Induction of NADPH cytochrome P450 reductase by the Alzheimer beta-protein. Amyloid as a "foreign body". *J Neurochem* 2001; **78**(1): 121-8.

61. Van Ess PJ, Pedersen WA, Culmsee C, Mattson MP, Blouin RA. Elevated hepatic and depressed renal cytochrome P450 activity in the Tg2576 transgenic mouse model of Alzheimer's disease. *J Neurochem* 2002; **80**(4): 571-8.

62. Shah BR, Xu W, Mraz J. Cytochrome P450 1B1: role in health and disease and effect of nutrition on its expression. *Rsc Adv* 2019; **9**(36): 21050-62.

63. Falero-Perez J, Song YS, Sorenson CM, Sheibani N. CYP1B1: A key regulator of redox homeostasis. *Trends Cell Mol Biol* 2018; **13**: 27-45.

64. Falero-Perez J, Song YS, Zhao Y, Teixeira L, Sorenson CM, Sheibani N. Cyp1b1 expression impacts the angiogenic and inflammatory properties of liver sinusoidal endothelial cells. *PLoS One* 2018; **13**(10): e0206756.

65. Palenski TL, Gurel Z, Sorenson CM, Hankenson KD, Sheibani N. Cyp1B1 expression promotes angiogenesis by suppressing NF-kappaB activity. *Am J Physiol Cell Physiol* 2013; **305**(11): C1170-84.

66. Chen F, Castranova V, Li Z, Karin M, Shi X. Inhibitor of nuclear factor kappaB kinase deficiency enhances oxidative stress and prolongs c-Jun NH2-terminal kinase activation induced by arsenic. *Cancer Res* 2003; **63**(22): 7689-93.

67. Tang Y, Scheef EA, Wang S, et al. CYP1B1 expression promotes the proangiogenic phenotype of endothelium through decreased intracellular oxidative stress and thrombospondin-2 expression. *Blood* 2009; **113**(3): 744-54.

68. Yang Z, Li H, Tang Y, et al. CYP1B1 deiciency ameliorates learning and memory deficits caused by high fat diet in mice. *Am J Transl Res* 2019; **11**(4): 2194-206.

69. Markesbery WR. The role of oxidative stress in Alzheimer disease. *Arch Neurol* 1999; **56**(12): 1449-52.

70. Mondragon-Rodriguez S, Perry G, Zhu X, Moreira PI, Acevedo-Aquino MC, Williams S. Phosphorylation of tau protein as the link between oxidative stress, mitochondrial dysfunction, and connectivity failure: implications for Alzheimer's disease. *Oxid Med Cell Longev* 2013; **2013**: 940603.

71. Liu Z, Li T, Li P, et al. The Ambiguous Relationship of Oxidative Stress, Tau Hyperphosphorylation, and Autophagy Dysfunction in Alzheimer's Disease. *Oxid Med Cell Longev* 2015; **2015**: 352723.

72. Lambert JC, Ibrahim-Verbaas CA, Harold D, et al. Meta-analysis of 74,046 individuals identifies 11 new susceptibility loci for Alzheimer's disease. *Nat Genet* 2013; **45**(12): 1452-8.

73. Jansen IE, Savage JE, Watanabe K, et al. Genome-wide meta-analysis identifies new loci and functional pathways influencing Alzheimer's disease risk. *Nat Genet* 2019; **51**(3): 404-13.

74. Steele NZ, Carr JS, Bonham LW, et al. Fine-mapping of the human leukocyte antigen locus as a risk factor for Alzheimer disease: A case-control study. *PLoS Med* 2017; **14**(3): e1002272.

75. Sasaki A, Kawarabayashi T, Murakami T, et al. Microglial activation in brain lesions with tau deposits: comparison of human tauopathies and tau transgenic mice TgTauP301L. *Brain Res* 2008; **1214**: 159-68.

76. Scheff SW, Price DA, Schmitt FA, DeKosky ST, Mufson EJ. Synaptic alterations in CA1 in mild Alzheimer disease and mild cognitive impairment. *Neurology* 2007; **68**(18): 1501-8.

77. Polydoro M, Acker CM, Duff K, Castillo PE, Davies P. Age-dependent impairment of cognitive and synaptic function in the htau mouse model of tau pathology. *J Neurosci* 2009; **29**(34): 10741-9.

78. Yin Y, Gao D, Wang Y, et al. Tau accumulation induces synaptic impairment and memory deficit by calcineurin-mediated inactivation of nuclear CaMKIV/CREB signaling. *Proc Natl Acad Sci U S A* 2016; **113**(26): E3773-81.

79. Hoover BR, Reed MN, Su J, et al. Tau mislocalization to dendritic spines mediates synaptic dysfunction independently of neurodegeneration. *Neuron* 2010; **68**(6): 1067-81.

80. Zhou L, McInnes J, Wierda K, et al. Tau association with synaptic vesicles causes presynaptic dysfunction. *Nat Commun* 2017; **8**: 15295.

81. Popugaeva E, Vlasova OL, Bezprozvanny I. Restoring calcium homeostasis to treat Alzheimer's disease: a future perspective. *Neurodegener Dis Manag* 2015; **5**(5): 395-8.

82. Kurbatskaya K, Phillips EC, Croft CL, et al. Upregulation of calpain activity precedes tau phosphorylation and loss of synaptic proteins in Alzheimer's disease brain. *Acta Neuropathol Commun* 2016; **4**: 34.

83. Tan Y, Deng Y, Qing H. Calcium channel blockers and Alzheimer's disease. *Neural Regen Res* 2012; **7**(2): 137-40.